AGU ADVANCING EARTH AND SPACE SCIENCE

Geophysical Research Letters

RESEARCH LETTER
10.1029/2021GL093265

Key Points:

- global simulations with resolved convection produce more realistic equatorial waves than simulation with parameterized convection
- it is not the horizontal resolution *per se* that matters, but the fact that convection is resolved instead of parameterized
- global models with resolved convection can improve tropical weather forecasts and climate projections relative to current-generation models

Supporting Information:

Supporting Information may be found in the online version of this article.

Correspondence to:

F. Judt,
fjudt@ucar.edu

Citation:

Judt, F., & Rios-Berrios, R. (2021). Resolved convection improves the representation of equatorial waves and tropical rainfall variability in a global nonhydrostatic model. *Geophysical Research Letters*, *48*, e2021GL093265. https://doi.org/10.1029/2021GL093265

Received 8 MAR 2021
Accepted 30 JUN 2021

Resolved Convection Improves the Representation of Equatorial Waves and Tropical Rainfall Variability in a Global Nonhydrostatic Model

Falko Judt[1] **and Rosimar Rios-Berrios**[1]

[1]National Center for Atmospheric Research, Boulder, CO, USA

Abstract Numerical weather and climate models continue to struggle with simulating equatorial waves and tropical rainfall variability. This study presents a potential remedy—high-resolution global models with explicitly resolved convection. A series of global nonhydrostatic simulations was produced with horizontal cell spacings between 3.75 and 480 km; the share of resolved precipitation in these simulations ranged from 88% to 2%. The simulations in which convection was mostly resolved produced much more realistic equatorial waves than the simulations in which convection was mostly parameterized. Consequently, the simulations with resolved convection produced more realistic precipitation patterns and precipitation variances. The results demonstrate that high-resolution global models with explicitly resolved convection are a promising tool to improve tropical weather forecasts and climate projections.

Plain Language Summary Despite frequent complaints that weather forecasts are more often wrong than right, weather prediction is actually one of science's big success stories. However, even though weather forecasts have generally become more accurate, forecasts in the tropics are indeed quite poor. The computer models that form the basis of modern weather prediction struggle with simulating tropical weather phenomena such as equatorial waves—weather disturbances that travel along the equator and bring alternating periods of rain and dryness. We demonstrate that the models' handling of equatorial waves can be much improved by increasing the model resolution, that is, by changing the models so that they can simulate the atmosphere in more detail. Specifically, the distance between grid cells must be made small enough so that the models can capture the building blocks of equatorial waves: individual showers and thunderstorms (a typical thunderstorm measures only 10 km or so in the horizontal direction). Once the models are able to capture these individual storms, they are able to produce much more realistic equatorial waves, and in turn, much better forecasts of tropical rainfall. The downside is that much larger computers with increased power consumption are necessary to accommodate the more detailed models.

1. Introduction

Numerical weather and climate models continually improve from one generation to the next, but even the most recent models struggle with simulating the tropical atmosphere in a realistic and useful way (e.g., Vogel et al., 2018). In particular, the models have difficulties with capturing equatorial waves—phenomena that modulate the wind and rainfall patterns in the tropics and influence the region's weather on timescales from days to weeks. Most climate model have been severely lacking in equatorial wave activity (Lin et al., 2006). This deficiency is not limited to coarse-resolution climate models; it plagues numerical weather models with 10–15 km grid spacing, too: In the 2015–2016 version of the operational Global Forecasting System (GFS), equatorial waves were found to decay shortly after model initialization, and as a result, the simulated rainfall patterns in the tropics become unrealistically stationary (Dias et al., 2018). In the present study, we demonstrate that models with explicitly resolved convection rather than parameterized convection produce more realistic equatorial waves and rainfall patterns.

Model studies indicate that convection parameterization is one—if not the—dominant reason for the deficiencies in current weather and climate models. Nakajima et al. (2013) and Rios-Berrios et al. (2020) demonstrate that the characteristics of equatorial waves are strongly affected by model formulation (of which

convection parameterization is a crucial aspect), to the point that different models with different convection schemes produce completely different wave modes and precipitation patterns. Bengtsson et al. (2019) showed that the poorly performing GFS from the Dias et al. (2018) study produces more realistic rainfall patterns once the model's native cumulus parameterization scheme has been replaced by a different one. In climate models, the amplitude of equatorial waves is sensitive to the convective trigger (Lin et al., 2008), and wave activity can be enhanced by strengthening the convective trigger (Frierson et al., 2011) or by suppressing convection until some threshold humidity in the the cloud layer is reached (Suzuki et al., 2006).

Given the ambiguities associated with the parameterization of convection, one may assume that simulating convection explicitly is better than parameterizing it. And indeed, some climate models produce more wave activity when the convection parameterization is turned off (Lin et al., 2008), even though doing so is generally not appropriate when the grid spacing is around 100 km. Conversely, turning off convection parameterization may be appropriate when the grid spacing reaches the "gray zone" for deep convection (somewhere in the 5–15 km range). Regional "storm-resolving" models (i.e., limited-area models with gray-zone resolution that explicitly resolve convective storms) were found to simulate equatorial waves quite realistically (Wang et al., 2015; Ying & Zhang, 2017). The literature is, however, lacking a conclusive demonstration that resolved convection leads to a better representation of equatorial waves in global models, mostly because of the tremendous computational resources that are needed to run and analyze global storm-resolving simulations. So far, studies in this area have been of the proof-of-concept type (Satoh et al., 2008) or limited by marginal horizontal resolution (e.g., Kodama et al., 2015; Miyakawa et al., 2014).

As computing power has been increasing, the limitations have been easing, and global storm-resolving models with grid spacings ≤5 km are beginning to enter the scientific main stream (Satoh et al., 2019; Stevens et al., 2019). Consequently, it becomes possible to more definitively assess the benefit of resolved convection in global atmosphere models. The present study intends to be part of this assessment; specifically, we evaluate the simulated precipitation patterns, equatorial wave activity, and the variance of precipitation in simulations that vary in grid spacing and whether or not convection is resolved or parameterized. Note that we merely wish to demonstrate the benefit of resolved convection; in other words, we are not concerned with the question of why resolved convection improves the representation of equatorial waves.

One of the limitations of this study is that we only analyze one model and one set of 40-days long simulations. Nevertheless, the results are quite clear and likely valid for other models, too. Finally, even though we use the term "resolved convection", convection is not fully resolved at the cell spacings considered here (a few kilometers). Yet, for clarity, we prefer the term "resolved convection" over more scrupulous constructs such as "permitted", "allowed", or "under-resolved convection".

2. Data and Methods

This study uses 10 simulations that were produced with the Model for Prediction Across Scales-Atmosphere (MPAS-A), a nonhydrostatic atmosphere model designed for meso- and cloud-scale as well as climate applications (Skamarock et al., 2012). The simulations were made for the "DYnamics of the Atmospheric general circulation Modeled On Non-hydrostatic Domains" (DYAMOND) initiative—the first intercomparison of global storm-resolving models—and follow the protocol detailed in Stevens et al. (2019). As such, the simulations were initialized with the 0000 UTC August 1, 2016 analysis from the European Center for Medium-Range Weather Forecasts (ECMWF) and integrated for 40 days (August 1–September 10, 2016). The sea surface temperature and sea ice fields were prescribed with 7-days running mean analyses from ECMWF.

The 10 simulations only differ in horizontal resolution and cumulus parameterization scheme. Concretely, the first eight simulations were produced on meshes with the following globally quasi-uniform cell spacings: 3.75 km, 7.5 km, 15 km, 30 km, 60 km, 120 km, 240, and 480 km. These eight simulations use an experimental scale-aware version of the new Tiedtke cumulus parameterization scheme (github.com:weiwangncar/MPAS-Model.git, branch "scale-aware"). All simulations use the same vertical discretization (75 levels, model top at 40 km).

The 3.75-km and 7.5-km simulations were repeated with the default ("full") new Tiedtke scheme (Zhang & Wang, 2017). The latter two simulations will be referred to as "full CP" to distinguish them from their

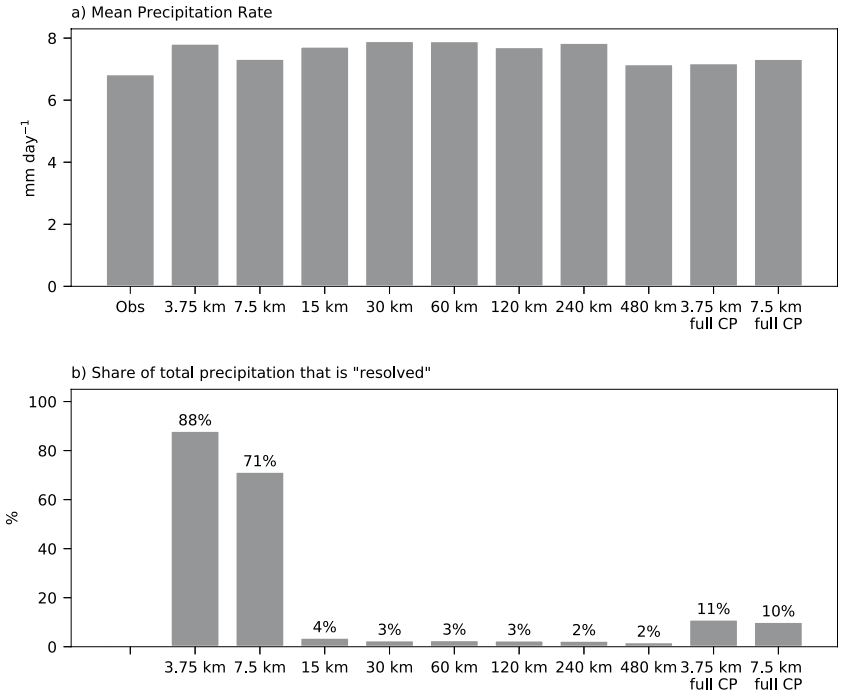

Figure 1. Area and time averaged precipitation rate (a), and share of total precipitation that is "resolved", that is, the share that is not produced by the cumulus parameterization scheme (b). Only data between 5°–15°N have been considered.

scale-aware counterparts. Simulations with cell spacings of ≥15 km were not repeated because the full scheme and the scale-aware scheme produce identical results for cell spacings ≥15 km.

The key assumption of scale-aware cumulus parameterization schemes is that, for a given horizontal resolution, a fraction of convection is resolved. Hence, there is a resolution-dependent partitioning of precipitation into a resolved and parameterized portion. Figure 1 shows the area and time averaged rainfall rate from observation and the 10 simulations, as well as the fraction of resolved precipitation for our 10 simulations (only grid cells between 5°–15°N have been considered). In the 3.75-km and 7.5-km simulations, convective storms are largely resolved, and the share of resolved precipitation is about 90% and 70%, respectively. Conversely, in the simulations with cell spacings between 15 and 480 km, convective storms are unresolved and the share of resolved precipitation is under 5%. Although the resolution of the two full CP runs would allow for the explicit simulation of convective storms, only about 10% of the precipitation is resolved; in other words, most of the precipitation in the full CP runs is produced by the cumulus parameterization despite their storm-resolving resolution.

We compared the simulations against observed rainfall estimates from the Integrated Multi-satellitE Retrievals for GPM (IMERG) version 6 data set (Huffman et al., 2019). The IMERG data, hereafter referred to as "observations", consist of gridded rain rates obtained from an algorithm that combines rainfall estimates from microwave satellites, microwave-calibrated satellites, and rain gauges. We used the "final run" product, which provides half-hourly rainfall rates with 0.1° resolution. The MPAS model, on the other hand, outputs accumulated rainfall. For a direct comparison, homogenization is necessary, and all precipitation data were first converted to 6-h accumulations and then interpolated to a common 2.5° latitude-longitude grid. Next, the gridded precipitation data were averaged in latitude between 5–15°N, yielding time-longitude precipitation arrays. Finally, we follow the approach of Wheeler and Kiladis (1999) and filter the time-longitude precipitation arrays in space and time to extract the equatorial wave signals. The implementation of the filtering method is the same as in Judt (2020).

3. Results

Hovmöller diagrams of unfiltered precipitation provide an overview of the near-equatorial rainfall patterns and allow for a cursory model evaluation (Figure 2). Clearly, the simulations in which convection is mostly resolved (Figures 2b and 2c) reproduced the observed rainfall patterns (Figure 2a) more accurately than the simulations in which convection is mostly parameterized (Figures 2d–2k). In fact, if one were to group the panels in Figure 2 into two sets based on overall similarity, one would presumably group the observations and the simulations with mostly resolved convection into one set, and the simulations with mostly parameterized convection into another set. In other words, the greatest dissimilarity is not between observation and simulation, but between observations and simulations with resolved convection ("set 1") on the one hand and simulations with parameterized convection ("set 2") on the other hand.

One of the differences between set 1 and set 2 involves rainfall intensity and the areal coverage of rainfall. In set 1, most of the rainfall is concentrated in locally confined areas where latitudinally averaged rainfall rates exceed 1.5 mm hr^{-1}. In set 2, precipitation is generally much lighter—rainfall rates are mostly under 1.5 mm hr^{-1}—but spread out over a much larger area. The overly expansive regions of light to moderate rain in set 2 and are almost certainly a manifestation of the notorious "raining too often but far too lightly" issue that plagues models with parameterized convection (e.g., Stephens et al., 2010). This issue is further illustrated in Figure 3. In comparison to set 1 (the blue and black lines), the simulations that belong to set 2 (the green and yellow lines) feature fewer grid points with latitudinally averaged rainfall rates above 1.0 mm hr^{-1}, more grid points with light rainfall rates between 0.03 and 0.5 mm hr^{-1}, and fewer grid points that are dry (leftmost bar, 0–0.015 mm hr^{-1}).

Another substantial difference between the two sets involves the propagation of the rainfall patterns. In set 1, most of the rainfall is associated with propagating features, some prominent examples of which are located between 0 and 45°W. In set 2, rainfall propagates to a much lesser degree, and the rainy areas in Figures 2d–2k appear unduly stationary and persistent, especially over the Indo-Pacific warm pool (90–180°E). This "stationarity bias" also seems to be an artifact of models with parameterized convection (see e.g., Dias et al., 2018, their Figure 1).

The combined information from Figures 1b and 2 suggests that the structure of the rainfall patterns—and hence the amount of agreement between simulation and observations—is determined by how much of the total precipitation is resolved, regardless of horizontal resolution. In support of this conclusion, note that the rainfall patterns in the 3.75 and 7.5-km full CP runs (Figures 2j and 2k) look more like the ones in the coarser resolution runs (Figures 2d–2i) than the ones in the 3.75 and 7.5-km runs (Figures 2b and 2c). Despite the differences in rainfall patterns, the simulations with resolved convection produced about the same amount of rainfall as the simulations with parameterized convection (Figure 1a). More precisely, all simulations produced area and time-averaged rainfall rates that were between 105%–116% of the observed rainfall rate, but a relationship between rainfall overproduction and resolution was not found (Figure 1a).

Although propagating features are evident in Figures 2a–2c, a direct relationship between these features and equatorial waves can only be revealed by wave-filtering, the result of which is presented in Figure 4. Figure 4f, for example, reveals that the previously mentioned prominent wave signals between 0 and 45°W are manifestations of tropical depression (TD)-type waves. Further circumstantial evidence, such as the time of year, geographic location and frequency suggest that these features are, in fact, African Easterly Waves.

Overall, the waves in the 3.75-km simulation (Figures 4b, 4g and 4l) best match the observations (Figures 4a, 4f and 4k). In fact, a quick glance does not reveal any meaningful differences in wave activity between the observations and the 3.75-km simulation, apart from the phase and amplitude differences associated with individual waves. This close agreement between observations and simulation is testimony to the ability of the storm-resolving MPAS-A to produce realistic equatorial waves.

The positive effect of resolving convection does not seem to be the same for all waves, however. Small-scale inertia-gravity waves feature the most pronounced change in activity when comparing the simulations with parameterized (Figures 4m–4o) and resolved convection (Figure 4l). Large-scale Kelvin waves, on the other hand, change comparatively little when transitioning from parameterized (Figures 4c–4e) to

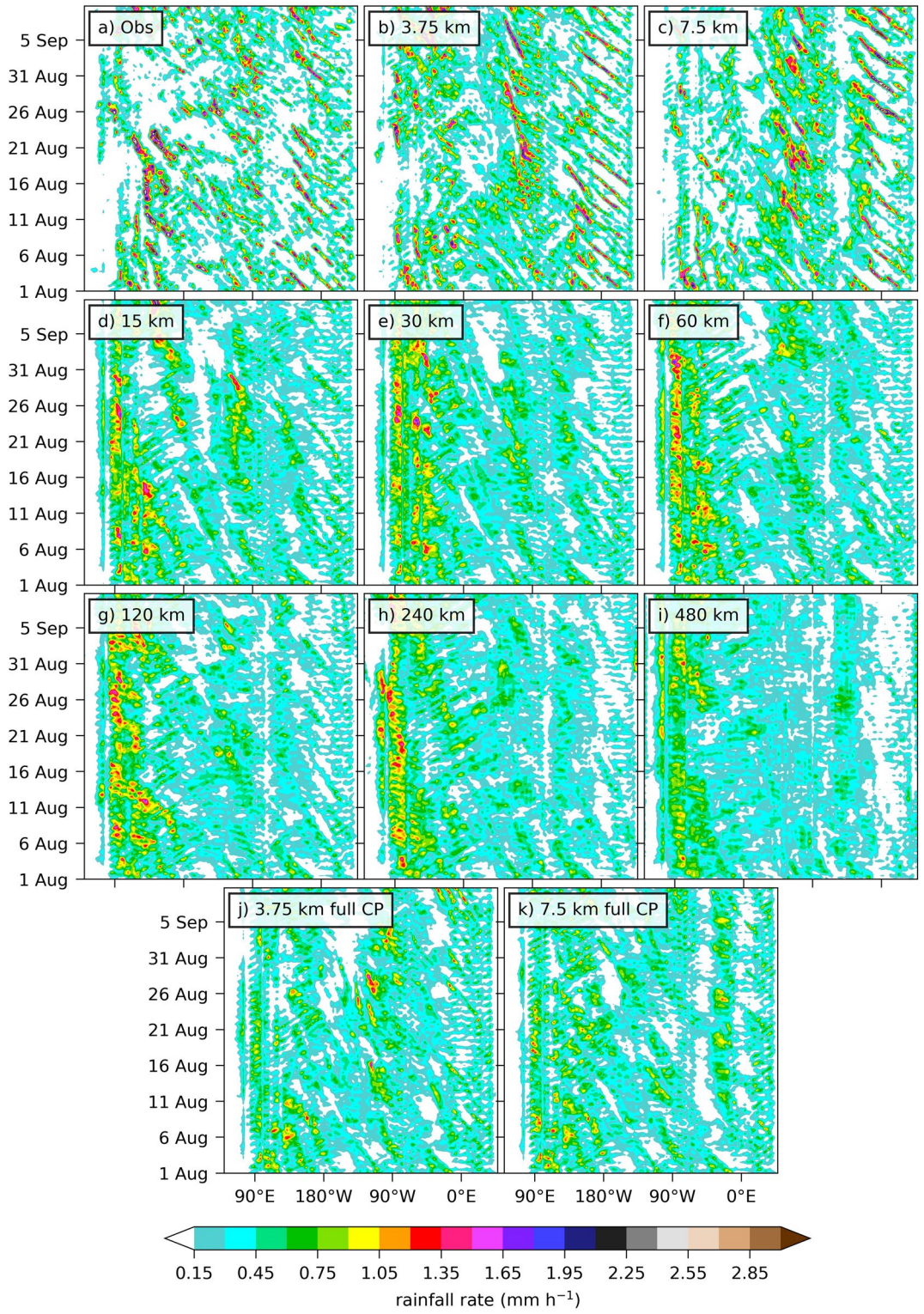

Figure 2. Hovmöller diagrams of latitudinally averaged (5–15°N) precipitation for the time period Aug 1–Sep 10, 2016. (a) IMERG observations; (b)–(k) MPAS simulations with cell spacings as indicated at the top of each panel; (j) and (k) are the same as (b) and (c), except they use the full new Tiedtke cumulus parameterization scheme instead of the scale-aware new Tiedtke scheme.

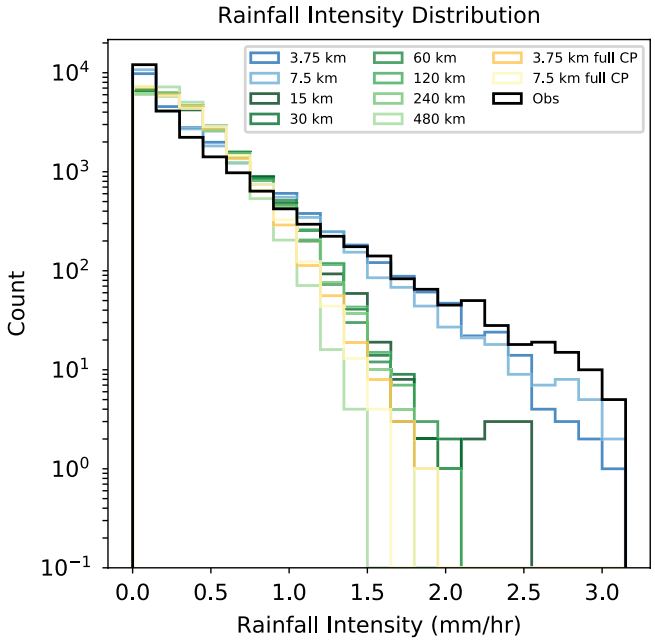

Figure 3. Histogram of rainfall intensity from observations (black) and simulations (colored lines). The figure presents the same data that is used to plot Figure 2, that is, the rainfall intensities are from the coarsened and latitudinally averaged data arrays. The bin width is 0.15 mm hr^{-1}, the same as the contour interval in Figure 2.

resolved convection (Figure 4b). For intermediate-scale TD-type waves, the change in activity is in between the two previously mentioned wave types (Figures 4h–4j vs. Figure 4g). We deduce from this behavior that the benefit of resolved convection is inversely related to the scale of the wave, or in other words, the positive effect of resolving convection is more important for smaller scale waves than for larger scale waves.

Although Kelvin waves are present in all simulations, the Kelvin waves in the 3.75-km run show the best agreement with observations in amplitude (Figures 4a and 4b). In the simulations with parameterized convection, the wave amplitude is smaller than in the observations, and the wave packets are less distinct (Figures 4c–4e). Nevertheless, the fact that even the 120-km MPAS simulated Kelvin waves supports Rios-Berrios et al. (2020), who demonstrated that MPAS-A is a "Kelvin-wave friendly" model in that the model develops robust Kelvin waves regardless of the choice of cumulus or other physical parameterization schemes.

Although smaller in scale than Kelvin waves, TD-type waves were a particularly active wave type during the experiment period (Figure 4f). Two areas of activity stood out: the western Pacific centered around 135°E and Africa/eastern Atlantic (45°E–45°W; these are the previously mentioned African Easterly Waves). The 3.75-km simulation captured the wave activity in the most realistic way (Figure 4g), whereas the simulations with parameterized convection struggled with reproducing the observed wave amplitudes (Figures 4h–4j). Nonetheless, even the 3.75-km simulation missed the peak of activity in the western Pacific east of 180°W.

Regarding $n = 1$ westward-propagating inertia-gravity waves, the simulations with parameterized convection do particularly poorly in reproducing the observed wave activity. The 3.75-km run, on the other hand, is much closer to the observations. Yet somewhat similarly, to the TD-type waves, the 3.75-km run misplaced the strongest activity: the observations suggest that the wave activity in the western Pacific and over Africa is roughly equally strong, while the simulation produces substantially stronger activity over Africa than over the western Pacific. A potential explanation for the higher-than-observed wave activity is that the model produces too strong of a West African monsoon.

To summarize and quantify the information contained in Figures 2 and 4, we followed the approach of Nakajima et al. (2013) and computed the variance of the 2D (time-longitude) precipitation fields. Results are shown both for unfiltered rainfall (Figure 5a) and for wave-filtered rainfall expressed as fraction of the total variance (Figure 5b). The bar plots uphold the results of the previous discussion and confirm that the 3.75-km simulation with resolved convection is closest to the observations. More precisely, the variance of the unfiltered rainfall from the 3.75-km simulation is 0.14 $mm^2\ hr^{-2}$, just 14% less than the observed value of 0.16 $mm^2\ hr^{-2}$. In contrast, the variance from the 15, 120, and 3.75-km full CP simulations is only about 0.06 $mm^2\ hr^{-2}$, that is, less than half of the observed value (Figure 5a).

The close agreement between the 3.75-km run and the observations also holds for the wave-filtered rainfall variance (Figure 5b). Summing the variances of Kelvin, TD-type, and inertia-gravity waves from the 3.75-km run yields 24% of the total variance—roughly the same as for the observations (22%). But not only the total sum of the variance is similar, the individual contributions from each wave type are similar, too. Specifically, in both the 3.75-km simulation and observations, 5%–6% of the total variance is contributed by Kelvin waves (dark blue), 10%–12% by TD-type waves (medium blue), and roughly 4%–5% by inertia-gravity waves (light blue).

The simulations with parameterized convection, on the other hand, are not able to generate the appropriate fractional contribution from TD-type and inertia-gravity waves (Figure 5b). Instead of the observed 10% (TD-type) and 5% (inertia-gravity), these two wave types only make up 5%–6% (TD-type) and a mere 1%

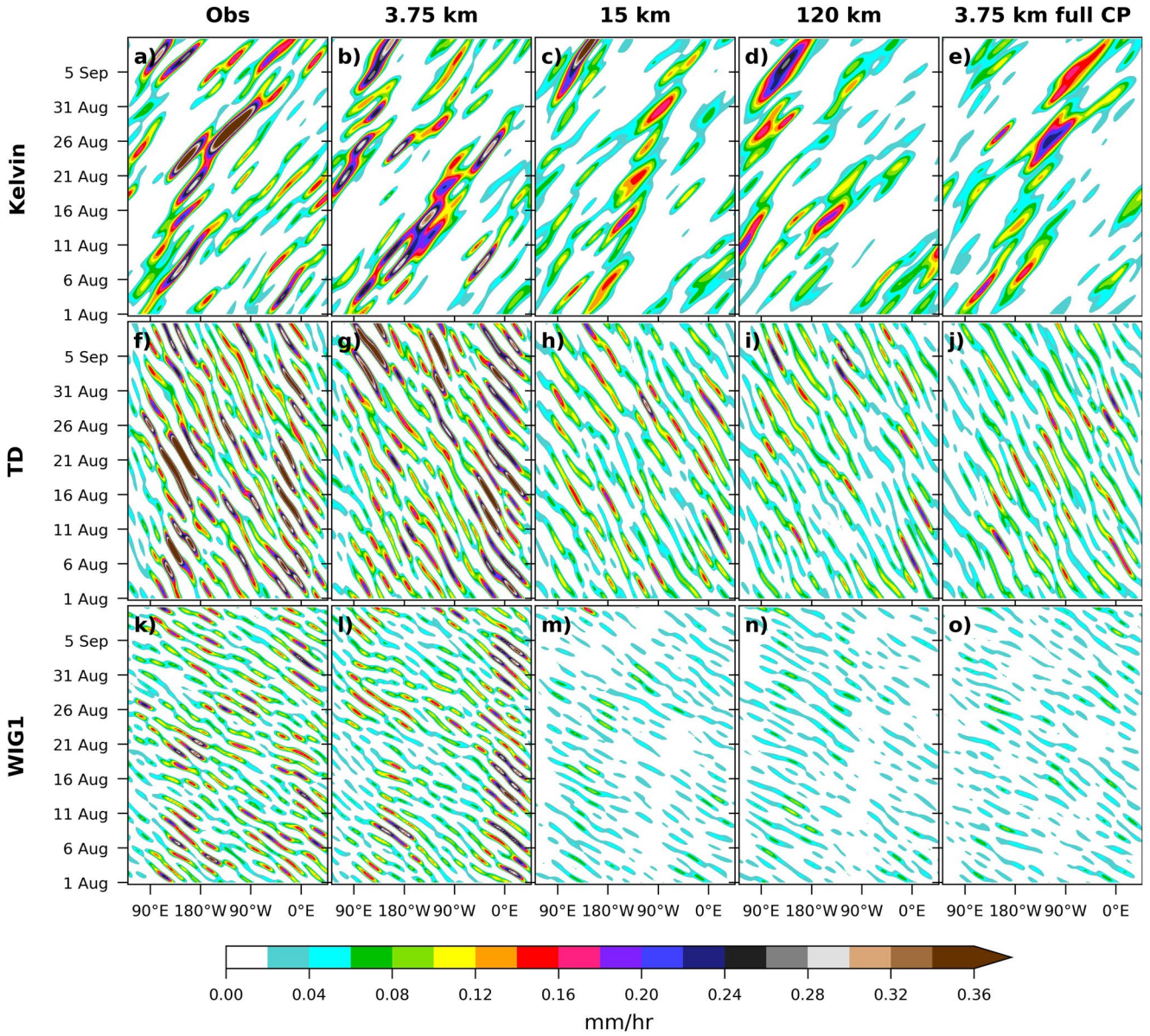

Figure 4. Hovmöller diagrams of wave-filtered precipitation for three wave types from observations (left column) and four Model for Prediction across Scales simulations (right four columns). (b), (g), (l) is from the 3.75-km simulation, (c), (h), (m) is from the 15-km simulation, and (d), (i), (n) is from the 120-km simulation. (e), (j), (o) is from the 3.75-km simulation that used the full new Tiedtke scheme. Top row shows Kelvin waves, middle row TD-type waves, and bottom row $n = 1$ westward-propagating inertia-gravity waves.

(inertia-gravity) of the total variance. It is worthwhile to emphasize that this deficiency comes on top of the inability to produce an adequate amount of variance to begin with (Figure 5a).

Figures 4 and 5 only presented results for a subset of the simulations and a subset of equatorial wave types. We chose the 3.75-km, 15, 120-km runs because their cell spacings represent, respectively, next-generation models with storm-resolving resolution, operational numerical weather prediction models, and current-generation climate models. We chose Kelvin, TD-type, and inertia-gravity waves because they represent large-scale, intermediate scale, and small-scale waves. Figures S1 and S2 in the Supplemental Material are similar to Figures 4 and 5 but include all 10 simulations and seven wave types (Kelvin, equatorial Rossby, mixed Rossby-gravity, TD-type, $n = 0$ eastward-propagating inertia gravity, and $n = 1$ as well as $n = 2$ westward-propagating inertia-gravity waves). Although more comprehensive, those figures tell a similar

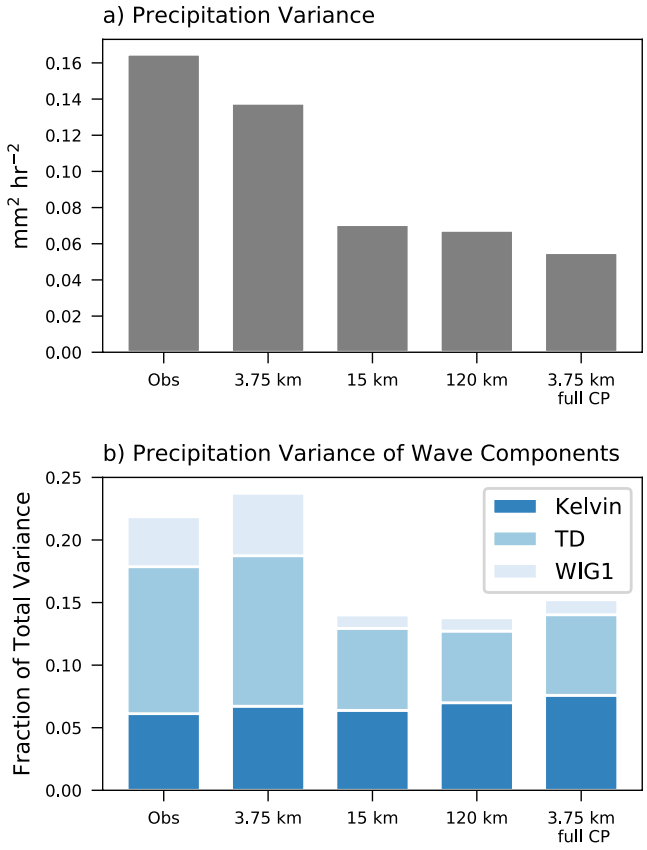

Figure 5. (a) Variance of precipitation from observations and four Model for Prediction across Scales simulations. (b) Variance of wave-filtered precipitation expressed as fraction of the total variance from the following wave types: Kelvin, tropical depression, and westward-propagating inertia-gravity.

story. One noteworthy result is that all wave types combined contribute roughly 40% to the total precipitation variance in the observations and between 29% and 40% in the simulations.

4. Summary and Conclusions

We used the global nonhydrostatic MPAS-A model to produce a series of simulations in which the share of resolved precipitation ranged from 88% (dx = 3.75 km) to 2% (dx = 480 km). On the basis of these simulations, we demonstrated that runs with (mostly) resolved convection developed more realistic equatorial waves than the simulations in which convection was (mostly) parameterized. As a consequence, the simulations with resolved convection produced more realistic rainfall patterns and rainfall variances. While resolving convection leads to more realistic wave activity across the board, the beneficial effect is inversely related to the scale of the equatorial wave type; in other words, resolving convection is more important for small-scale inertia-gravity waves than for large-scale Kelvin waves. We also found that it is not the horizontal resolution *per se* that matters, but the fact that convection is resolved instead of parameterized. Although the results are quite clear, they may be different in a different model with a different convection scheme. Moreover, the analyses are fairly qualitative and based on a single 40 days period. Finally, the representativeness of the results is likely not uniform as waves with periods varying from 2–20 days are sampled differently in a 40 days long simulation.

The main actionable conclusion of this study is that tropical weather forecasts can be improved by making operational numerical weather prediction models "storm-resolving" (also referred to as cloud resolving, convection permitting or convection allowing). In particular, the grid spacing needs to be decreased so that convective storms can be explicitly resolved. This study suggests that 7.5 km is sufficient to produce realistic equatorial waves. Previous work suggested that even 10–15 km may be adequate for this purpose as long as convection is not parameterized (e.g., Kodama et al., 2015; Miyakawa et al., 2014; Wang et al., 2015). For other phenomena, a finer grid spacing may be needed. For example, accurately simulating tropical cyclone intensity requires a grid spacing of of 1–2 km (e.g., Fox & Judt, 2018; Gentry & Lackmann, 2010).

Of course, an increase in resolution leads to higher computational costs, but the potential benefits that result from more realistic equatorial waves—such as increasingly skillful rainfall forecasts and improvements in predicting tropical cyclone formation—may outweigh the additional costs. In fact, it may be possible to increase the predictability horizon of tropical weather forecasts beyond that of the middle latitude, as recent research suggests that equatorial waves have longer predictability than the baroclinic weather systems of the middle latitudes (Judt, 2020).

In closing, the present study highlights the seemingly intractable problems that arise from convection parameterization. Our results support the view of Stevens et al. (2019) in that the best way to evade these problems is to "explicitly simulate how small and intermediate scales of motions couple to large-scale circulation systems." We furthermore endorse Palmer and Stevens (2019) in that global storm-resolving models are better suited to answer the great science questions associated with climate change than current-generation models with parameterized convection.

Data Availability Statement

IMERG data were accessed via NASA's Goddard Earth Sciences Data and Information Services Center (https://disc.gsfc.nasa.gov/). The MPAS-A source code (Jacobsen et al., 2019) can be downloaded from https://doi.org/10.5281/zenodo.3241875. Other data necessary to reproduce the results are available in an NCAR Digital Asset Services Hub repository (Judt & Rios-Berrios, 2021), including the data files to create the figures and the namelist for the MPAS simulations (filename: namelist.atmosphere). To run MPAS with the setup used in this study, you need to download the MPAS code and replace the file module_cu_ntiedtke.F in/src/core_atmosphere/physics/physics_wrf with module_cu_ntiedtke.F from the repository before compilation (the file from the repository includes the experimental scale-aware version of the Tiedtke cumulus scheme). You also need the initial condition file which can be made available upon request (size: 444 GB). Then the simulations can be reproduced using the provided namelist.

Acknowledgments
The authors acknowledge high-performance computing support from Cheyenne (doi: 10.5065/D6RX99HX) provided by NCAR's Computational and Information Systems Laboratory. This material is based upon work supported by NCAR, which is a major facility sponsored by the National Science Foundation under Cooperative Agreement No. 1852977. The comments from two anonymous reviewers helped to improve the manuscript.

References

Bengtsson, L., Dias, J., Gehne, M., Bechtold, P., Whitaker, J., Bao, J.-W., et al. (2019). Convectively coupled equatorial wave simulations using the ECMWF IFS and the NOAA GFS cumulus convection schemes in the NOAA GFS model. *Monthly Weather Review*, *147*(11), 4005–4025. https://doi.org/10.1175/mwr-d-19-0195.1

Dias, J., Gehne, M., Kiladis, G. N., Sakaeda, N., Bechtold, P., & Haiden, T. (2018). Equatorial waves and the skill of NCEP and ECMWF numerical weather prediction systems. *Monthly Weather Review*, *146*(6), 1763–1784. https://doi.org/10.1175/mwr-d-17-0362.1

Fox, K. R., & Judt, F. (2018). A numerical study on the extreme intensification of hurricane Patricia (2015). *Weather and Forecasting*, *33*(4), 989–999. https://doi.org/10.1175/waf-d-17-0101.1

Frierson, D. M. W., Kim, D., Kang, I.-S., Lee, M.-I., & Lin, J. (2011). Structure of AGCM-simulated convectively coupled kelvin waves and sensitivity to convective parameterization. *Journal of the Atmospheric Sciences*, *68*(1), 26–45. https://doi.org/10.1175/2010jas3356.1

Gentry, M. S., & Lackmann, G. M. (2010). Sensitivity of simulated tropical cyclone structure and intensity to horizontal resolution. *Monthly Weather Review*, *138*(3), 688–704. https://doi.org/10.1175/2009mwr2976.1

Huffman, G. J., Bolvin, D. T., Nelkin, E. J., & Tan, J. (2019). *Integrated multi-satellitE Retrievals for GPM (IMERG) technical documentation*. National Aeronautics and Space Administration. Retrieved from https://docserver.gesdisc.eosdis.nasa.gov/public/project/GPM/IMERG_doc.06.pdf

Jacobsen, D., Duda, M., Petersen, M., Hoffman, M., Turner, A. K., ldfowler58, et al. (2019). *Mpas-dev/mpas-model: Mpas version 7.0*. Zenodo. Retrieved from https://doi.org/10.5281/zenodo.3241875

Judt, F. (2020). Atmospheric predictability of the tropics, middle latitudes, and polar regions explored through global storm-resolving simulations. *Journal of the Atmospheric Sciences*, *77*(1), 257–276. https://doi.org/10.1175/jas-d-19-0116.1

Judt, F., & Rios-Berrios, R. (2021). *Data for grl article "resolved convection improves the representation of equatorial waves and tropical rainfall variability in a global nonhydrostatic model"*. UCAR/NCAR - CISL - CDP. Retrieved from https://dashrepo.ucar.edu/dataset/211_fjudt.html. https://doi.org/10.5065/v05b-9e73

Kodama, C., Yamada, Y., Noda, A. T., Kikuchi, K., Kajikawa, Y., Nasuno, T., et al. (2015). A 20-year climatology of a NICAM AMIP-type simulation. *Journal of the Meteorological Society of Japan. Series II*, *93*(4), 393–424. https://doi.org/10.2151/jmsj.2015-024

Lin, J.-L., Kiladis, G. N., Mapes, B. E., Weickmann, K. M., Sperber, K. R., Lin, W., & Scinocca, J. F. (2006). Tropical intraseasonal variability in 14 IPCC AR4 climate models. Part I: Convective signals. *Journal of Climate*, *19*(12), 2665–2690. https://doi.org/10.1175/jcli3735.1

Lin, J.-L., Lee, M.-I., Kim, D., Kang, I.-S., & Frierson, D. M. W. (2008). The impacts of convective parameterization and moisture triggering on AGCM-simulated convectively coupled equatorial waves. *Journal of Climate*, *21*(5), 883–909. https://doi.org/10.1175/2007jcli1790.1

Miyakawa, T., Satoh, M., Miura, H., Tomita, H., Yashiro, H., Noda, A. T., et al. (2014). Madden–julian oscillation prediction skill of a new-generation global model demonstrated using a supercomputer. *Nature Communications*, *5*(1), 3769. https://doi.org/10.1038/ncomms4769

Nakajima, K., Yamada, Y., Takahashi, Y. O., Ishiwatari, M., Ohfuchi, W., & Hayashi, Y.-Y. (2013). The variety of spontaneously generated tropical precipitation patterns found in APE results. *Journal of the Meteorological Society of Japan. Ser. II*, *91A*, 91–141. https://doi.org/10.2151/jmsj.2013-a04

Palmer, T., & Stevens, B. (2019). The scientific challenge of understanding and estimating climate change. *Proceedings of the National Academy of Sciences*, *116*(49), 24390–24395. https://doi.org/10.1073/pnas.1906691116

Rios-Berrios, R., Medeiros, B., & Bryan, G. H. (2020). Mean climate and tropical rainfall variability in aquaplanet simulations using the model for prediction across scales-atmosphere. *Journal of Advances in Modeling Earth Systems*, *12*(10), e2020MS002102. https://doi.org/10.1029/2020ms002102

Satoh, M., Matsuno, T., Tomita, H., Miura, H., Nasuno, T., & Iga, S. (2008). Nonhydrostatic icosahedral atmospheric model (NICAM) for global cloud resolving simulations. *Journal of Computational Physics*, *227*(7), 3486–3514. https://doi.org/10.1016/j.jcp.2007.02.006

Satoh, M., Stevens, B., Judt, F., Khairoutdinov, M., Lin, S.-J., Putman, W. M., & Düben, P. (2019). Global cloud-resolving models. *Current Climate Change Reports*, *5*(3), 172–184. https://doi.org/10.1007/s40641-019-00131-0

Skamarock, W. C., Klemp, J. B., Duda, M. G., Fowler, L. D., Park, S.-H., & Ringler, T. D. (2012). A multiscale nonhydrostatic atmospheric model using centroidal voronoi tesselations and c-grid staggering. *Monthly Weather Review*, *140*(9), 3090–3105. https://doi.org/10.1175/mwr-d-11-00215.1

Stephens, G. L., L'Ecuyer, T., Forbes, R., Gettelmen, A., Golaz, J.-C., Bodas-Salcedo, A., et al. (2010). Dreary state of precipitation in global models. *Journal of Geophysical Research*, *115*(D24), D24211. https://doi.org/10.1029/2010jd014532

Stevens, B., Satoh, M., Auger, L., Biercamp, J., Bretherton, C. S., Chen, X., et al. (2019). Dyamond: The Dynamics of the atmospheric general circulation modeled on non-hydrostatic domains. *Progress in Earth and Planetary Science*, *6*(1), 61. https://doi.org/10.1186/s40645-019-0304-z

Suzuki, T., Takayabu, Y. N., & Emori, S. (2006). Coupling mechanisms between equatorial waves and cumulus convection in an AGCM. *Dynamics of Atmospheres and Oceans*, *42*(1–4), 81–106. https://doi.org/10.1016/j.dynatmoce.2006.02.004

Vogel, P., Knippertz, P., Fink, A. H., Schlueter, A., & Gneiting, T. (2018). Skill of global raw and postprocessed ensemble predictions of rainfall over northern tropical Africa. *Weather and Forecasting*, *33*(2), 369–388. https://doi.org/10.1175/waf-d-17-0127.1

Wang, S., Sobel, A. H., Zhang, F., Sun, Y. Q., Yue, Y., & Zhou, L. (2015). Regional simulation of the October and November MJO events observed during the CINDY/DYNAMO field campaign at gray zone resolution. *Journal of Climate*, *28*(6), 2097–2119. https://doi.org/10.1175/jcli-d-14-00294.1

Wheeler, M., & Kiladis, G. N. (1999). Convectively coupled equatorial waves: Analysis of clouds and temperature in the wavenumber–frequency domain. *Journal of the Atmospheric Sciences*, *56*(3), 374–399. https://doi.org/10.1175/1520-0469(1999)056<0374:CCEWAO>2.0.CO;2

Ying, Y., & Zhang, F. (2017). Practical and intrinsic predictability of multiscale weather and convectively coupled equatorial waves during the active phase of an MJO. *Journal of the Atmospheric Sciences*, *74*(11), 3771–3785. https://doi.org/10.1175/jas-d-17-0157.1

Zhang, C., & Wang, Y. (2017). Projected future changes of tropical cyclone activity over the western north and south pacific in a 20-km-mesh regional climate model. *Journal of Climate*, *30*(15), 5923–5941. https://doi.org/10.1175/jcli-d-16-0597.1